Acta Biomaterialia 9 (2013) 4826–4835

Contents lists available at SciVerse ScienceDirect

Acta Biomaterialia

journal homepage: www.elsevier.com/locate/actabiomat

Direct evidence for continuous linear kinetics in the low-temperature degradation of Y-TZP

M. Keuper *, K. Eder, C. Berthold, K.G. Nickel

Eberhard Karls University Tübingen, Faculty of Science, Department of Geosciences, Applied Mineralogy, Wilhelmstraße 56, 72074 Tübingen, Germany

ARTICLE INFO

Article history:
Received 4 May 2012
Received in revised form 23 July 2012
Accepted 20 August 2012
Available online 24 August 2012

Keywords:
Zirconia
Low temperature degradation
Bioceramics
Phase transformation
TZP

ABSTRACT

The kinetics of the tetragonal to monoclinic (t–m) transformation of zirconia in a hydrous environment at 134 °C and 3 bar pressure was studied. As surface X-ray diffraction, which is conventionally used to explore the progress, has a very limited depth of information, it distorts the quantitative results in a layer-on-layer situation and by itself is ill suited for this reason. Analyzing cross sections is more suitable; therefore, focused ion beam techniques were used to prepare artifact-free cuts. The material was subsequently investigated by scanning electron microscopy, electron backscatter diffraction and Raman spectroscopy. Only the combination of methods makes it possible to resolve the quantifiable details of the process. The transformation starts in the near-surface areas, forms a layer, and the growth of this layer proceeds into the bulk material following a simple linear time law (0.0624 μm h^{-1} for material in the chosen condition), without apparent retardation or limit. The progress yields a gradientless layer with a fixed amount of residual tetragonal zirconia (~27% for 3Y-TZP in the present conditions) separated from unaffected material by a boundary, which has a roughness only in the grain size range. The kinetics indicates a reaction rate control, where the hydration reaction is the key factor, but is modified by the stepwise access of water to the reaction front opened by the autocatalytic transformation of zirconia with a critical hydration level.

1. Introduction

The transformation in Y-TZP from tetragonal to monoclinic (t–m) zirconia, with both benefits regarding the mechanical properties and possible problems for the application, lifetime prediction is a well-known and controversially discussed phenomenon. In recent times, many publications have dealt particularly with the degradation phenomena at low temperatures (e.g., Refs. [1–3]). At low or moderate temperatures, the t–m transformation process can be initiated by mechanical treatment [4–8] or under the influence of water and/or its vapor [1,2,9,10]). Guo [11] and Lawson [12] provided good overviews of the influence of water or water vapor (see also Refs. [3,13,14]).

To quantify the progress of the transformation with time, X-ray diffraction (XRD) or, to a minor extent, Raman spectroscopy are mostly used. The increase in monoclinic zirconia as a function of both time and temperature, as calculated from XRD analyses of hydrothermally altered material, was commonly interpreted to follow a sigmoidal trend. This shape led to kinetic models for the transformation process, which were based on the Mehl–Avrami–Johnson (MAJ) law [15]. As early as 1965, Whitney [16] described a kinetic MAJ model for ZrO_2 and the nucleation and growth process prevailing during transformation. In 1987, Lu et al. [17] reported a sigmoidal trend to describe transformation processes occurring in autoclaved zirconia in an air atmosphere and explained it by a transformation pace decreasing with time. A logarithmic aging function for samples stored under humid conditions was deduced. In contrast, Lilley [1] and Lawson and Smith [18] proposed the time-dependence of transformation to be a linear process. They suggested that the transformation has no incubation time and that "the phase transformation reaches saturation immediately and grows inwards linearly with time" [12].

Thus, they proposed a simpler model for the growth process of the monoclinic phase, although their work provided only indirect analytical proof.

More recently, most interpretations have gone back to the initial MAJ model. For example, Gremillard et al. [19] and Cattani-Lorente et al. [20] used the MAJ approach to differentiate between a nucleation-dominated or growth-controlled transformation process in a model for the aging kinetics of zirconia.

The MAJ law thus became widely accepted and can be divided into three successive states: (i) an initial state, where single and isolated tetragonal grains or nuclei at the surface begin to transform into the monoclinic structure; (ii) an exponential increase in the monoclinic phase, which is commonly interpreted as a

* Corresponding author. Tel.: +49 7071 2976805; fax: +49 7071 293060.
E-mail address: Melanie.keuper@uni-tuebingen.de (M. Keuper).

1742-7061/$ - see front matter © 2012 Acta Materialia Inc. Published by Elsevier Ltd. All rights reserved.
http://dx.doi.org/10.1016/j.actbio.2012.08.032

3-dimensional growth of the monoclinic phase into the volume; and (iii) a "saturation phenomenon", as described in the work of Nakajima et al. [21], for example; according to these authors the transformation does not increase further after reaching a certain amount of monoclinic phase in the near-surface area. This "saturation" is caused by the maximum transformable tetragonal phase content. In the case of the 3Y-TZP material with the distinct composition and grain size used in the present study, the maximum monoclinic amount is ~70 wt.% [3,20,22–31]. It should be mentioned that this maximum monoclinic amount can vary, depending on the grades of the material (cf., Ref. [31]), but the fact that even a maximum transformed material never attains 100% m-ZrO_2 applies accordingly to all material compositions. This is attributed to internal compressive stresses [1] induced by the volume expansion of the monoclinic structure, which inhibits transformation of statistically distributed residual tetragonal grains or clusters [20].

The transformation front in a MAJ model is commonly viewed as a gradual decrease in monoclinic ZrO_2 within the transformation layer from the surface into the interior of the sample. Consequently, no distinct border between transformed and unaffected material should be visible, but there should be a smooth transition. Marro et al. [23] showed that XRD data can be interpreted to be consistent with a smooth transition. Cattani-Lorente et al. suggested this additionally as an exponential, gradual decrease [20]. In contrast, Wada and Yokoyama argue that the transformation decreases linearly with depth [27].

However, the assumption of a gradual transition was challenged in several studies: Recent work by Muñoz-Tabares et al. [24] proposed a non-linear gradient in the in-depth distribution of the monoclinic phase based on Raman spectroscopy. These authors found that the monoclinic phase content remained constant over a longer distance until a "sharp drop" occurred, after which the concentration decreased slowly with increasing depth. Similarly, Kim et al. [32] stated that the transformation front is fully transformed "a little far away from the interface between the degraded and the intact layer", and that the amount of m-ZrO_2 is gradually reduced in this small region between a near-interface region within the transformation and interface itself because of microstructural effects.

Thus, the shape of the boundary between altered zirconia and the virgin material remains a subject of controversy and, if the boundary is indeed a sharp one instead of gradual, then the kinetics of the process may also have to be reinterpreted. To resolve this problem, the only practicable way is to look for direct evidence, which comes from cross sections of the transformed region prepared by a gentle preparation method such as focused ion beam (FIB) milling, followed by combined characterization techniques such as scanning electron microscopy (SEM), electron backscatter diffraction (EBSD) and μ-Raman spectroscopy, which is the subject of the present work.

This study focuses on just one material, a 3 mol.% Y_2O_3 TZP, which is typical for dental materials. Whether the findings are true for other materials and aging conditions should be investigated in further studies.

2. Experimental

Pre-sintered rectangular white bodies of yttria-doped tetragonal zirconia material (VITA InCeram YZ, 3 mol.% yttria (3Y-TZP); VITA Zahnfabrik Rauter, Bad Saeckingen, Germany) with a small alumina content <0.3 wt.% were sintered for 2 h at 1530 °C, yielding a dense ceramic body ($\rho = 6.05\ g\ cm^{-3}$) with a median grain size in the sub-micrometer range. The sintered samples with the dimensions of ~11 × 11 × 5 mm did not receive any further surface treatment after the sintering process. Up to three samples for each aging time and reference were chosen to evaluate the uncertainties.

Sintered samples were analyzed by XRD and Raman spectroscopy, where only tetragonal ZrO_2 was detected. With an alumina content <0.3 wt.%, these methods do not allow detection of dissolved alumina or aluminous phases. XRD pattern analysis by Rietveld refinement gave no evidence for the presence of cubic zirconia.

The sintered samples were hydrothermally aged by placing them in an autoclave directly after the sintering process (SANOclav, Bad Ueberkingen-Hausen, Germany) under a humid atmosphere at 134 °C and saturated water vapor pressure of 3 bar for storage times between 3 and 200 h. For comparison, similar prepared samples were used, stored in dry atmosphere at room temperature for equal times.

The bulk samples were characterized by X-ray microdiffraction with a Bruker D8 Discover GADDS θ/θ microdiffractometer equipped with a Co-sealed tube, a HOPG-primary monochromator, 500 μm monocapillary optic with 300 μm pinhole (IFG Berlin Adlershof, Germany) and a 2-dimensional VÅNTEC-500 area detector covering 40°2θ and psi (μ-XRD^2) [33].

The relative vertical analyzing depth of XRD in a material, in the present case a surface layer, depends on the incidence angle of the X-ray beam if the wavelength of the anode material and the mass attenuation coefficient of the material remain unchanged. Owing to the θ/θ setup used, the incidence angle can be chosen independently of the detector. Therefore, the analyzing depth can be modified via the incidence angle. Incidence angles between 1° and 10° result with the present setup in penetration depths between ~0.4 and ~4.2 μm, calculated with 99% of absorption in the material with the Lambert–Beer law [34] (see Eq. (1)). But it must be kept in mind that, on the one hand, the result is always a mean value of the entire excitation volume with exponential decrease of information with increasing depth and, on the other hand, the real information depth depends strongly on the diffracted intensity of the individual reflection that is analyzed.

For the first information regarding the time- and depth-dependent amount of monoclinic zirconia in the subsurface region during the aging process, the bulk samples were measured with incidence angles varying from 1° to 10° and a detector angle varying between 39° and 30° to ensure always measuring the same 2θ range.

The amounts of monoclinic ZrO_2 were then calculated using the commonly accepted formula of Garvie and Nicholson [35] modified by Toraya et al. [36], which gives information about the volume fraction v_m of the m-phase. To verify any interpretation from analytical methods, insight into the transformed subsurface areas was obtained from local cross sections taken from those samples. This is commonly done by mechanical cutting, grinding and polishing processes, but for ZrO_2-materials it is well known that mechanical treatment induces the t–m transformation [4–8]. Therefore, the investigation of mechanically prepared samples does not allow one to distinguish between the transformations due to the aging process and those due to the following preparation step.

To overcome this disadvantage, the cross sections were prepared and characterized via a combined FIB/SEM system AURIGA®–CrossBeam® Workstation (Carl Zeiss NTS GmbH, Oberkochen, Germany) with a Ga-ion beam and a field emission (FE) cathode at the NMI (Natural and Medical Sciences Institute at the University of Tübingen). Previous studies [37,38] confirmed that the milling conditions chosen did not cause any artificial transformation or re-transformation.

A limitation of this method is the low maximum depth of the trench cut into the sample surface by FIB in a reasonable time. To overcome this, the geometry of the section was modified by milling the samples on an edge at an angle of 45° (Fig. 1). In this

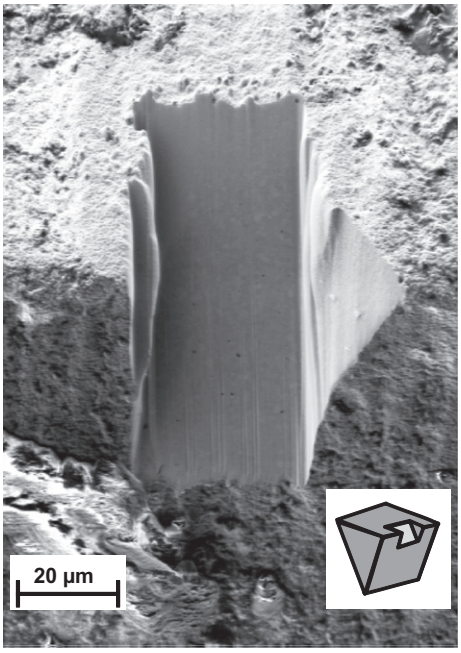

Fig. 1. SEM micrographs and schematic drawing (insert) of the FIB-milled diagonal cross section on an edge of a sample.

way, the visible spatial resolution on the section is increased, and the statistics are optimized.

Thus, two transformed surfaces were exposed, on the upper and lower sites, and the unaffected material in the middle of the cross section. The real depth of any investigated spot on the diagonal cross section was recalculated geometrically. The cross section had dimensions $\sim 20 \times 50$ µm, which is large enough for further investigations such as µ-Raman spectroscopy and EBSD.

The microstructure of the samples was studied by FE-SEM. Phase analysis was made by Raman spectroscopy using a confocal Raman spectrometer with a laser wavelength of 532 nm and WiRE 3.3 software (Renishaw InVia Reflex, Gloucestershire, UK).

Additionally, the phase distribution was characterized in detail by EBSD (FE SEM Leo 1560 VP, Carl Zeiss NTS GmbH, Oberkochen, Germany, with an EBSD detector and associated HKL Flamenco software from Oxford Instruments, Tubney Woods, Abingdon, Oxfordshire, UK) at the Institute for Materials Science at the University Stuttgart Germany. To get a convincing result, the compliance of each phase with the structures in the database was set to be >85%. Collected data with less compliance resulted in white data points, and hence the mean angular deviation was too high.

3. Results

3.1. XRD-measurements

3.1.1. XRD measurements with incidence angle fixed at 10°

µ-XRD[2]-patterns (10° incidence angle) of sample surfaces aged for 3–200 h are shown in Fig. 2. It is obvious that the intensity of monoclinic phase increases with increasing aging time. After 72 h of storage, no further decrease in the tetragonal main reflex and no increase in the monoclinic reflexes can be investigated. Quantifying these patterns by calculating the volume fractions of monoclinic ZrO_2, the typical time-dependent behavior, commonly described as sigmoidal, is shown in Fig. 3. The error bars come from the mathematical fitting error (χ^2) of the reflex pattern analyses and are in the range of ~3% of the calculated data. This corresponds well with the typical sample-to-sample variation of ~±4%.

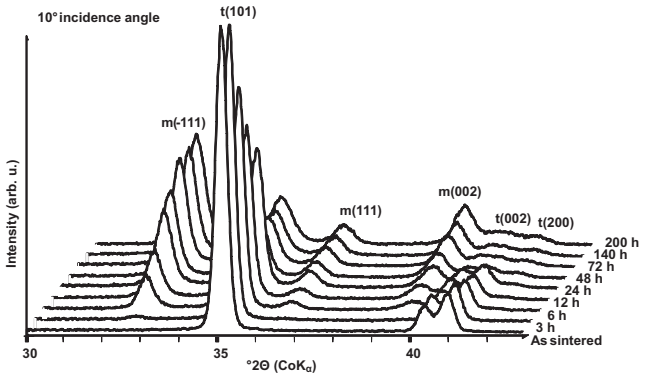

Fig. 2. Surface µ-XRD data from 10° fixed incidence angle of the aged samples after various storage times (listed on the right side) in hydrothermal atmosphere at 134 °C. Reflexes from monoclinic and tetragonal zirconia faces are marked with m and t, respectively.

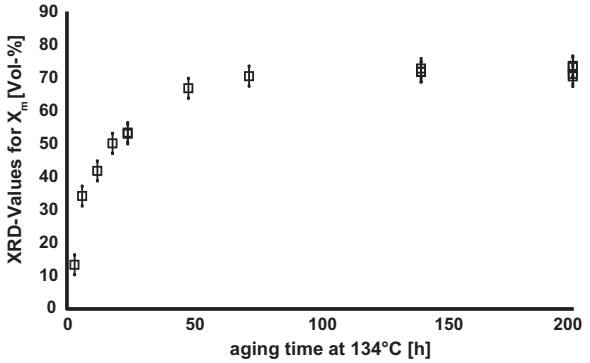

Fig. 3. Quantified data from the XRD surface measurements with 10° fixed incidence angle. The initial increase in the monoclinic phase fraction shows the typical exponential curvature and "saturation" with no apparent further increase in monoclinic phase after ~72 h.

An initial incubation/activation is possible but statistically insignificant and extends at most to a few hours, followed by strong growth of monoclinic zirconia. After ~72 h, no further increase is detectable, and the typical maximum amount of monoclinic ZrO_2 of 73% in 3 mol.% Y_2O_3 TZP is reached. Therefore, the present data agree with previous work [21,24,27]; after a certain aging time, no further increase in the monoclinic phase amount is detected. But owing to the fixed incidence angle and therefore the limited analyzing depth at this point, no definite statement regarding the spatial development of the monoclinic phase within the transformed layer is possible.

3.1.2. XRD measurements with incidence angles ⩽10°

Fig. 4 compares the results from measurements with differing fixed incidence angles. The maximum monoclinic amount (~73%) is approached at smaller incidence angles even in samples altered for shorter times.

The interpretation of the data is not completely unambiguous. However, from the values at 1° incidence, it is clear that the very surface down to 400 nm has reached the saturation level of 73% monoclinic phase already at a time of 12 h. And the data from 10° on samples exposed for 72 h and longer also have definitive results: The complete section documented has reached this 73% level. However, the depth of the section is ~4 µm at a 10° incidence angle, and thus the result does not indicate whether the layer continues to greater depths or not.

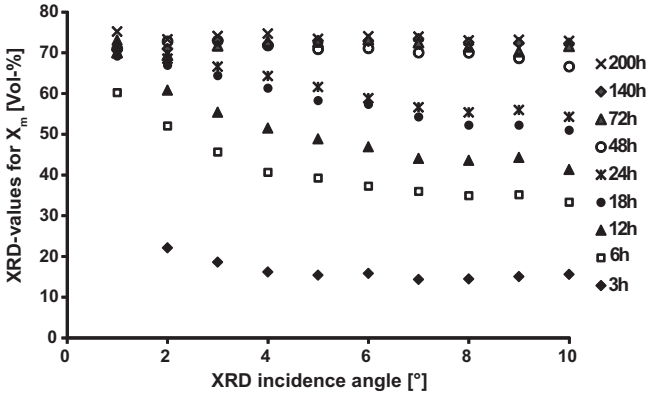

Fig. 4. Quantified data from the μ-XRD surface measurements as a function of the incidence angle ⩽10°, which corresponds to increasing analyzing depths. Low angle data from near-surface areas show that the saturation level of monoclinic amount is already reached after 12 h of hydrothermal storage.

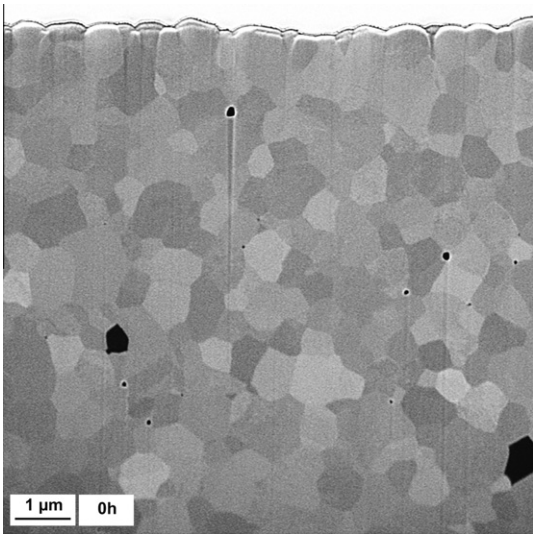

Fig. 5. SEM micrograph of a FIB-milled cross section of an as-sintered sample without further treatment, showing a fully dense and homogeneous microstructure without any indication of a t–m transformation.

The remainder of the data in Fig. 4 allow a number of interpretations: either they reflect a distribution of intermediate amounts of monoclinic phase in the whole section down to the individual penetration limit (and several distribution patterns would be possible); or they reflect a layer of constant monoclinic amount (i.e., 73%) growing in thickness and including a thickness exceeding the penetration depth at longer times of hydrothermal aging.

3.2. SEM

As the FIB preparation is a time-consuming (~6 h) and expensive way to prepare cross sections, not all the aged samples, which were characterized by XRD, were used to prepare cross sections for detailed characterization of the microstructure. Some specific samples were chosen, with aging times of 24 h, 48 h, 140 h and 200 h, along with an unaltered reference sample.

To confirm that there is no influence of the preparation method on the sample, a cross section of the sample without further hydrothermal treatment (0 h) was prepared via FIB directly after the sintering (cf., Ref. [38]). Surface analyses by XRD before the FIB milling process gave no evidence for monoclinic ZrO_2 on the surface or in the subsurface region.

The SEM view of the cross section (Fig. 5) reveals a dense microstructure without cracks extending from the direct surface to the deeper interior. The absence of twinning in the grains supports the finding that no transformation at all occurred during preparation.

Detailed characterization of the cross section by Raman spectroscopy also gave no evidence of any monoclinic amount, either in the subsurface region or in the bulk material.

From these results, it is clear that FIB milling is an ideal tool for preparing cross sections of ZrO_2 without inducing a transformation process in the prepared area.

In contrast to Fig. 5, in all the FIB-milled cross sections of the hydrothermal aged samples (Fig. 6) a zone of differing appearance was observed, reaching from the surface down to some depth into the bulk material. Within this zone, most of the ZrO_2 grains exhibit a microstructure within the individual grain, which is interpreted to reflect the typical twinning caused by the martensitic transformation to the monoclinic structure. Only a few grains within this layer seem to be unaffected.

With longer aging time, this transformed zone expands deeper into the interior of the sample. The interface is not completely flat, as it follows grain boundaries of the original microstructure on a small scale and roughly the surface profile on a somewhat larger scale. It is important to point out that the interface between unaffected and transformed material thus always shows a distinct border without any gradual decrease and has a fairly precise thickness. Additionally, distinct cracks could be observed in this region, beginning after 48 h of hydrothermal aging (Fig. 6b). They run nearly parallel to the surface, which is in accordance with optical investigations in other work [24,39,40].

To obtain information about the real thickness of the sample, it must be kept in mind that the analyzed FIB cross section is not perpendicular to the surface. Owing to the modified preparation procedure, the cross section has an angle of 45° with respect to the surface. Therefore, the measured thickness of the layer from the SEM picture must be converted by an angle correction of $\sqrt{2}/2$.

The measured depth of the transformed zone of each aging time is, as mentioned above, almost constant, with an error in the range of the grain size, in the present case ~0.8 μm. After 24 h, the transformed layer has a real thickness (corrected from the diagonal cross section to the observed depth; see Fig. 6a) of ~1.8 μm (this corresponds on the SEM-picture ~2.5 μm). After 48 h, the real layer thickness is ~3.5 μm, after 140 h ~8.3 μm and after 200 h 12.6 μm (Fig. 6d). From these optical observations, one can conclude that the thickness of the transformed layer increases linearly with time (Fig. 7) at a rate of 0.0624 μm h^{-1}.

3.3. EBSD mapping and Raman spectroscopy

To confirm that the martensitic twinning observed by SEM is indeed caused by the transformation to monoclinic zirconia, μ-Raman spectroscopy and EBSD were used.

To investigate the transition region from transformed to unaffected material with EBSD, a 200-h-aged sample was chosen. The results are shown in Fig. 8, in which it is plain that the monoclinic phase is the main phase present in the previously observed regions with twinning features. Some residual tetragonal grains are present in this area, which corresponds well to the information from XRD. Again, the sharp border to the zone of tetragonal zirconia in the bulk material is visible, with no gradual decrease in between.

In the core zone with tetragonal zirconia, the grains appear to be decorated by monoclinic rims. It is not certain whether this is due to a structural distortion of rims in general, which causes the program to interpret these parts as transformed or ill identifiable,

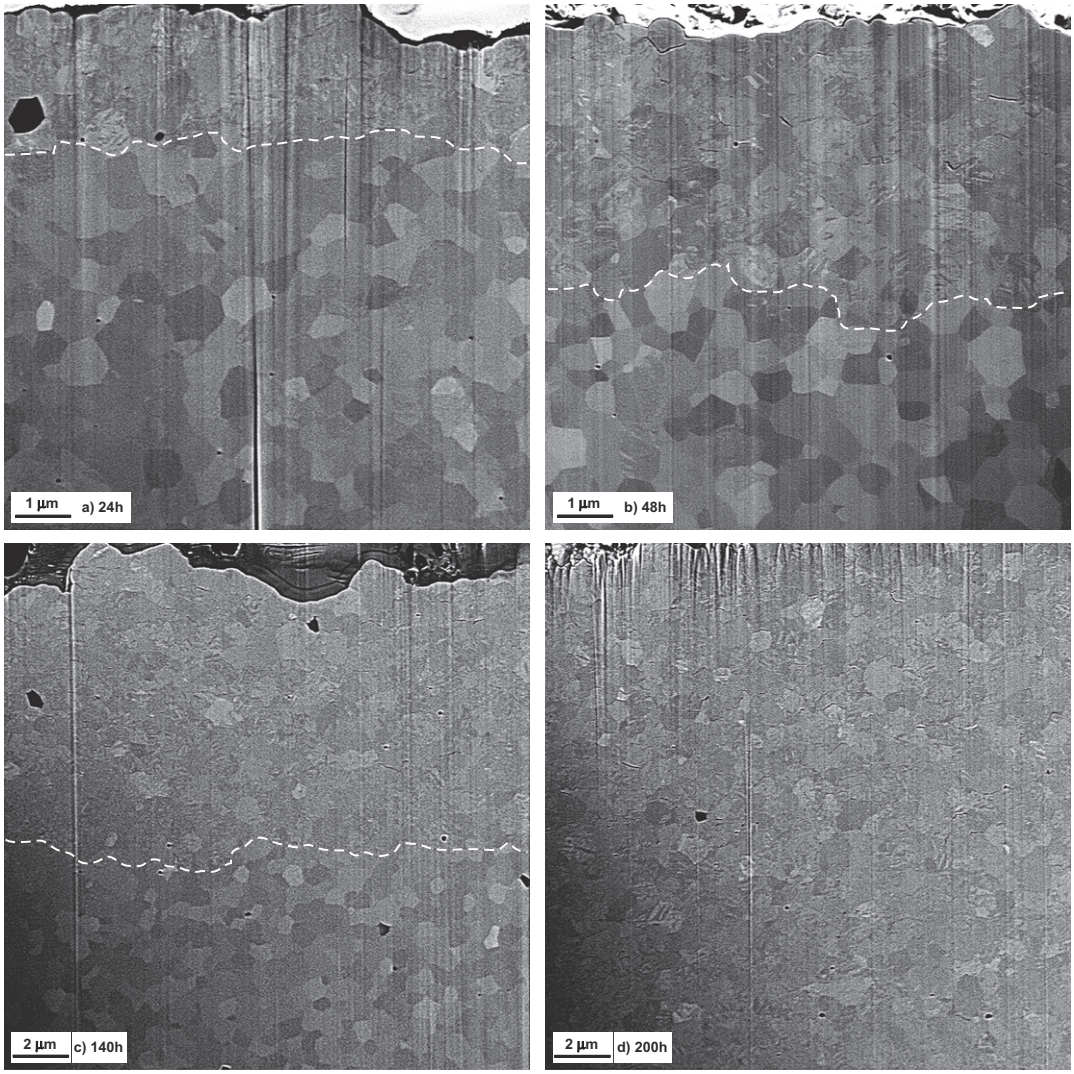

Fig. 6. SEM micrographs of the cross sections (45° cut) after different times of hydrothermal storage. The dashed line highlights the border between transformed (twinning visible) and virgin material. Note that the displayed depth of the transformation front has to be recalculated to yield the true vertical depths of 1.8 µm, 3.5 µm and 8.3 µm in (a), (b) and (c), respectively. The depth of ~12.6 µm for the condition of (d) has overrun the visible section.

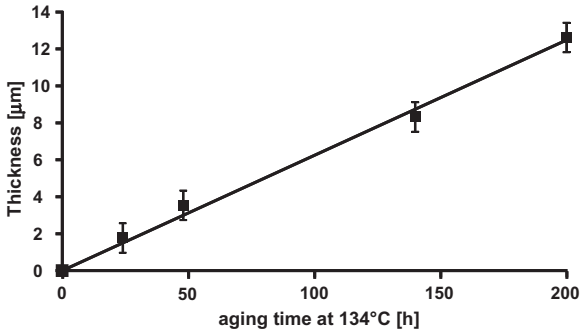

Fig. 7. Transformed layer thickness determined in FIB cuts (cf., Fig. 6) as a function of storage times at 134 °C. A linear rate constant of 0.0624 µm h^{-1} (=1.5 µm day^{-1}) is obtained with $r^2 > 0.98$. Error bars correspond to the microstructure with a grain size of ~800 nm.

or whether this is indeed a transformed rim, but due to the transport of the section, exposing it to moist air. Without further clues from careful studies, the evidence points rather towards a clear-cut grain-to-grain boundary.

Additionally, the FIB-milled area of each specimen was measured by Raman spectroscopy. In Fig. 9, a typical mapping by µ-Raman spectroscopy of the 140-h-aged sample is shown. The border between the untransformed and transformed zone is again clearly detectable and in very good agreement with the SEM results and also with the EBSD measurements. The visible gradient of the monoclinic intensities directly at the sharp border is an artifact of analysis, as discussed below.

4. Discussion

4.1. Raman spectroscopy and the transition shape

In Fig. 9, Raman spectroscopy seems to indicate a gradual change over ~20 µm in the transition between transformed and unaffected zirconia. This is a measurement artifact caused by the geometry of the analyzed volume. As shown in greater detail in previous studies [41–43], the zone, from which information is gathered in confocal Raman spectroscopy is not confined to the focal point. The double cone of penetrating rays together with pathway-length-dependent absorption creates an information zone, which, for the case of the optically transparent zirconia and the

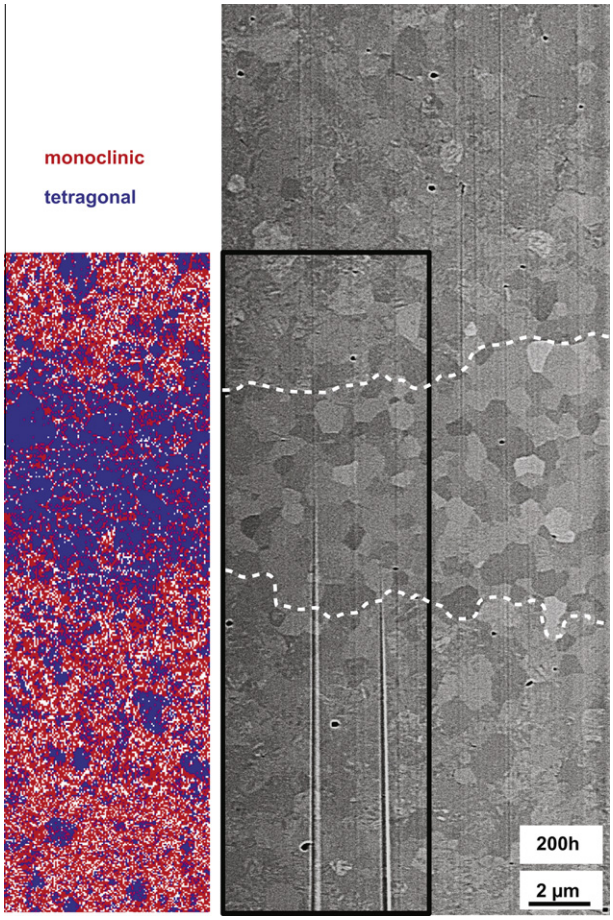

Fig. 8. SEM micrograph indicating the location (rectangle) of the EBSD map to the left of it. The sample was autoclaved for 200 h at 134 °C. Areas identified as tetragonal zirconia are shown in black (blue), monoclinic in gray (red). Areas of non-identified phases are shown in white. The border of the transformation front obviously coincides with the border to twinned grains in the SEM micrograph.

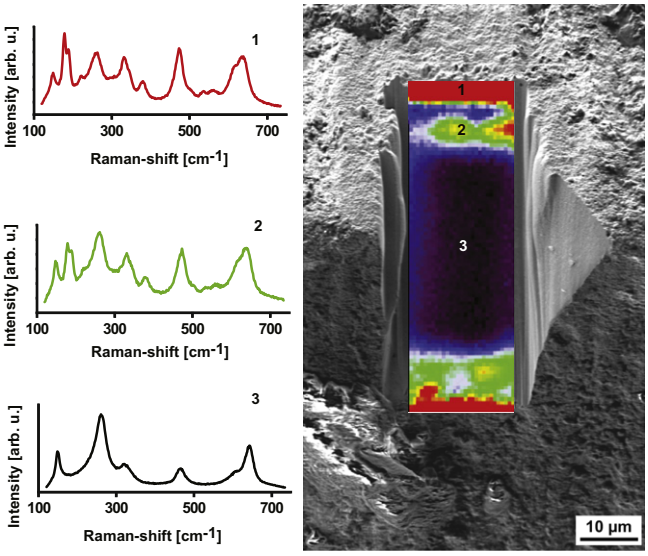

Fig. 9. Raman-mapping of the cross-section of a sample after 140 h at 134 °C. No monoclinic signals are shown in black (3), and strong monoclinic signals are shown in dark gray /red (1), exemplified by representative Raman spectra left to the points marked on the map.

present laser wavelength, extends to several tens of microns into the material, despite a focal area only 1 µm diameter. This is depicted schematically in Fig. 10, where the resulting phenomenon for the present cut edge is visible: a sharp boundary will occur as a blurred edge, because the spectra contain varying amounts of information from the underlying zone.

Taking this into account, the results of Muñoz-Tabares et al. [24] may be reinterpreted to support the present findings of a sharp edge. The recent study of Wulfman et al. [30] similarly showed a plateau in the monoclinic amount in the measured volume after 90 h of aging in Ringer solution at 130 °C. The authors calculated a homogeneous degree of 80% v_m for the Raman spectroscopy measurements, extending up to 20 µm after this aging time. They guessed, but did not study, the nature of the interface to the unaffected material. The interpretation of a maximum in monoclinic phase at ~2.5 µm seems not to fit the result above and may be due a focus problem, because the absolute intensities from micro-Raman studies always have a maximum when focusing slightly inside the sample—another effect of the analyzing volume here (see also Dorn et al. [44]).

4.2. XRD of a sharp moving boundary

Previous works stated a maximum transformation depth of 11 µm [8] and 6 µm [20], respectively, combined with an exponential decrease in the first few micrometers [20], hence a gradual appearance of the monoclinic layer. Another work stated a thickness of the degraded layer of 6 ± 2 µm, based on Raman spectroscopy measurements on cross sections [24].

The work of Gaillard et al. [45] determined the thickness via FIB cross sections on degraded material, similarly to the present work. They showed that the thickness of the layer depends on the material and the grain size, but their maximum investigated depth of the transformation was ~6 µm. Chowdhury et al. [26] stated a dependence between monoclinic fraction in mole per cent and layer thickness, although the equation used for the quantification from Ref. [35] is based on volume per cent. This resulted in a maximum of transformation of 78 mol.% of monoclinic zirconia. At this stage, the layer reaches a thickness of up to 8 µm.

All these studies reflect a transformation depth for a specific storage time of the samples, but are not evidence for a maximum depth of the layer.

Depth profiling from XRD data was discussed by Gremillard et al. [46], who explicitly mentioned the absorption problem discussed below. A consequence of this problem is that correct values are obtained if these patterns are deconvoluted appropriately. However, this is impossible without knowledge on the character of the interface (gradient or sharp boundary) and the character of the transformed layer.

The present investigations do provide this information, and thus the sigmoidal trend of the development of the monoclinic phase amounts in Fig. 3 is seen as the result of a distorted averaging phenomenon. XRD integrates over the whole measured volume, and a moving boundary will simply record differing ratios of a mixture of the upper and lower layer. However, the additional distortion comes from the changing absorption: the X-rays, which detect the lower layer, are more strongly absorbed on the way to the layer and back to the detector, because there is an exponential increase in absorption with depth, which is described by the Lambert–Beer law:

$$I/I_0 = \exp(-\varepsilon c d) \quad (1)$$

where I is intensity in/out, ε is the extinction coefficient, c is the concentration, and d is the penetrated thickness.

The apparent saturation limit of the sigmoidal curve is then approached, when only one homogeneous transformed layer is

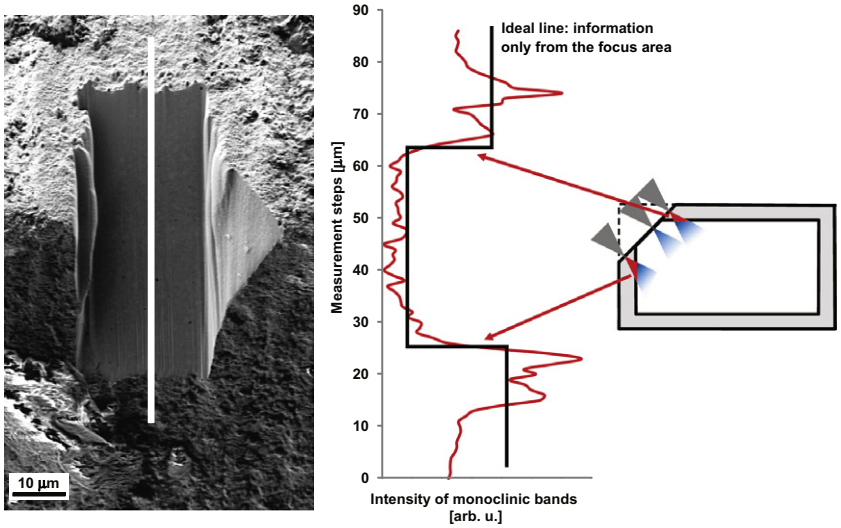

Fig. 10. SEM micrograph of a diagonal cross section of a 140 h autoclaved sample indicates the position of a Raman line scan of relative intensities of the monoclinic main bands. The sketch figure on the right-hand side illustrates that the seemingly blurred transition in the scan is caused by the interplay of sample geometry and laser excitation volume.

present up to the maximum X-ray analyzing depth. The value of this limit thus expresses a reality: the saturation of a volume of zirconia that will not transform further because of residual stresses. This coincides with previous work [19,23,31,45]. The transformation front, however, continues to move ahead underneath the ascertainable volume of the X-ray beam.

This is demonstrated by the samples after 140 h and 200 h, where XRD shows no further increase in the monoclinic amount. But in the cross sections (Fig. 6), a further proceeding of the transformation into the bulk material is clearly visible.

4.3. Kinetics of alteration

The three states of the MAJ law are consequently explained by methodical limitations of the individual analytical method used. The first stage, the nucleation period, is possibly a physical reality for the transformation in zirconia in other materials or conditions, but not necessarily to explain the data here. In agreement, Lawson [12] already stated in 1995 that there is no significant incubation time at 134 °C for this material. Whether 3Y-TZP with differing grades has different transformation rates or shows real incubation periods is not the focus of this study, but a subject for future work. However, the recent work of Kosmač and Kocjan [31] strongly points towards this. Other studies, which observed long incubation periods at lower temperatures (e.g., Chevalier [9]) should be discussed together with the mounting data sets in the literature, but this is outside the context of the present paper.

From the discussions above, it is clear that surface XRD data of 3Y-TZP at 134 °C cannot distinguish artifact from reality. The "exponential growth period" of the MAJ model has to be interpreted as the distorted consequence of a linear layer-growth combined with the Lambert–Beer law, as already analyzed by Lawson [12].

Some of the data from literature can now be reinterpreted within the picture of a continuously growing transformation layer: Marro et al. [23] reported a layer thickness of ~1.2 µm after a 10 h annealing time, which correlates perfectly with the present experiments. Lilley [1] reported a layer thickness of >100 µm after hydrothermal aging at 120 °C for 1000 h. In the study by Lepistö and Mäntylä [47], the "layer was so thick that it delaminated from the surface" after 2000 h of annealing at 150 °C.

Thus, the present authors believe that other studies and data on other materials involving zirconia are also to be interpreted to reflect simple linear layer growth kinetics. A detailed discussion of the literature and authors' own results will be published elsewhere. It should be noted that it is very likely that material (type and concentration of stabilizer, impurities and additives such as alumina), structural (grain sizes) and environmental details (e.g., P_{H_2O}, P_{total}) are most likely to change the rate constant and possibly the transformation limits. It is beyond the effort of this study to evaluate this.

4.4. Modeling the aging kinetics

The discussion above leaves the question of whether and how surface XRD data can be used to infer true kinetics. An obvious choice would be the deconvolution of the data. However, the penetration depth of the X-ray beam, or more precisely the detection depth of the diffracted signal, depends on several factors, such as wavelength (energy) and primary flux of the X-ray beam, detector sensitivity, incidence and diffracted angle. Accurate values for I_0 intensities will thus be hard to obtain.

To interpret the data, the data set must be split into two parts: at the time when the maximum monoclinic amount has been reached, not only is the value of the residual tetragonal detected,

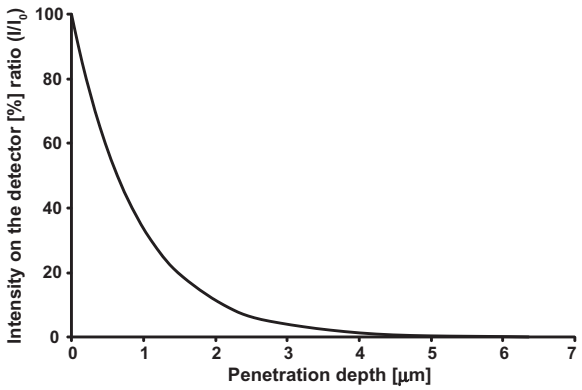

Fig. 11. Detected signal Intensity ratio (I/I_0) (%) as a function of the depth, from which the signal is created. Values were calculated for ZrO_2 with 10° incidence angle and Co K_α radiation in reflective mode.

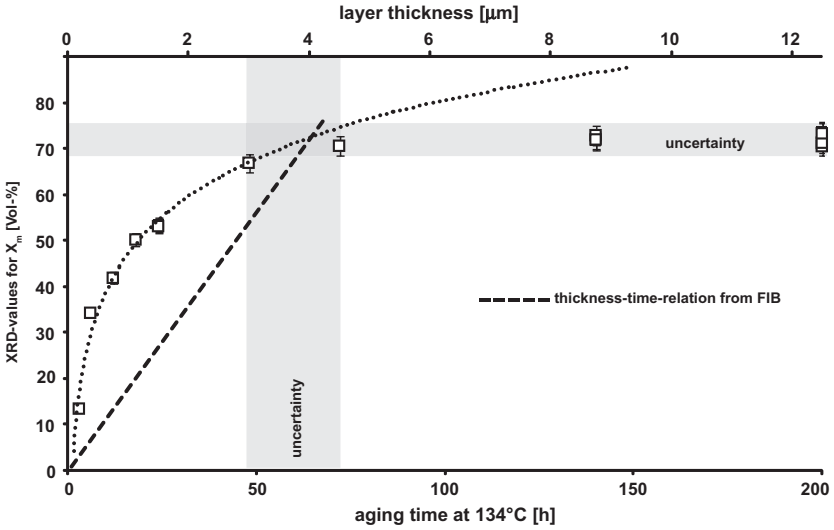

Fig. 12. Monoclinic volume fraction as calculated from XRD (10° fixed incidence angle) as a function of autoclave storage time. Top *x*-axis indicates the thickness of the transformed layer as calculated from the rate constant of Fig. 7. The fitted ln(*x*) function (dotted line) is a good approximation of the calculated data only up to the vertical gray shaded uncertainty time. The horizontal gray shaded uncertainty area comes from the constant maximum monoclinic fraction determined after a long time exposure. The uncertainty areas meet at values corresponding to the coincidence of transformed layer depth and maximum analyzing depth of the XRD setup used.

but it must coincide with the detection limit for the X-ray-condition used. In the present sample material and instrument setup (Co K_α radiation, reflective mode: 10° incidence angle and the area detector at 30° therefore covering a range from ~20° to 60° 2θ) the maximum analyzable layer thickness was attained after 48–72 h (Figs. 3 and 12). At this time, the FIB study with the rate constant of 0.0624 µm h^{-1} from Fig. 7 indicates a layer thickness of 3–4.5 µm. This correlates well with the maximum penetration depth calculated in the classical way according to the Lambert–Beer law (see Eq. (1)). Fig. 11 shows the remaining intensity on the detector with respect to the penetration depth. Most of the detected signal derives from the first 4 µm (regarding the setup with Co K_α radiation and an incidence angle of 10°).

From the data derived above (Fig. 12), i.e., the time the maximum analyzing depth coincides with the constant value of monoclinic fraction, one may already derive a kinetic value, because without a significant incubation period, the linear kinetics go straight through the origin, and the rate constant is calculated simply by dividing the analyzing depth by this time.

The second method for deriving a linear rate constant from XRD data is also the consequence of the absorption problem: regardless of the correctness of the calculated values of the volume fraction, one must follow formally the exponential function of the Lambert–Beer law. Therefore, the section of data, until the analyzing depth is reached, must have the mathematical form:

$$X_m = k \ln(t) \quad (2)$$

X_m describes the monoclinic amount, t is the storage time, and k is a constant.

The value of k is not of interest here unless one wants to deconvolute the data physically. But once the analyzing depth is reached, the calculated data for X_m will no longer follow the curve according to Eq. (2). When the correlation breaks down, there is a second clue to the time for layer thickness to coincide with the analyzing depth. This is shown in Fig. 12 as well. Similarly, this time–thickness point is a straight reflection of a rate constant in the absence of a nucleation period.

A positive check or verification of the rate constant is then obtained by preparing just one FIB section from a sample near this critical point.

Kosmač and Kocjan [31] also used cross sections for gaining the real transformation depth into the material and compared these results with their XRD data. They used Cu K_α radiation, penetrating deeper into the material. Consequently, they should see their maximum transformable monoclinic amount at a later stage of aging, corresponding to the maximum penetration depth of their XRD setup.

4.5. Transformation nucleation

The EBSD-measurements show a distinct border between transformed and unaffected material. The unaffected material, hence the tetragonal region, shows indications for some monoclinic zirconia mainly on grain boundaries. The appearance of this phase on the present sections is attributed to a storage time between the FIB milling and the analyses by EBSD, during which they were exposed to external influences.

Monoclinic zirconia distributed around the grains could be interpreted as the appearance of nuclei as envisaged in several models [11]. It would favor a scenario described by Tsukuma [48], who argued for a start at the grain boundaries (see Ref. [47]) and a further development into the grain center with time.

This is certainly not the whole story, because in the investigated transformed layer one sees either transformed grains or untransformed grains and no sign of partially transformed grains with accordingly thick rims. The linear increase in the transformed zone with time, and thus with a constant transformation rate, which was also noted by Lilley [1], Lepistö et al. [47,49] and Lawson [18] indicates a non-diffusion controlled process such as an "autocatalytic" self-propagating transformation [24]. Lepistö et al. [49] reported the enrichment of OH^- ions only in the surface of humid aged samples as detected by XPS, so they concluded that these ions nucleate the t–m transformation. However, they showed that OH^- ions do not extend throughout the transformed layer, and interpreted this as evidence for an autocatalytic process "without the requirement of continued hydroxyl ion involvement".

The emerging idea for the process would then involve an unimpeded penetration of water constituents in the transformed layer—which seems plausible in view of the cracks formed—and a kinetic control by the reaction velocity of these water constituents with the surface of the zirconia grains. Once a critical value is reached,

the grain transforms completely, exposing the next grain to the wet condition. All in all, linear kinetics then prevail.

5. Conclusions

The present results, especially the investigation of the FIB cross sections via SEM and EBSD, present direct evidence of the transformation behavior after different aging times. It is shown that the transformation process from tetragonal to monoclinic ZrO_2 under hydrothermal conditions (134 °C/3 bar saturated water vapor pressure) in 3 mol.% Y-TZP produces a well-defined region of monoclinic ZrO_2 with amounts of ~73%. The layer itself expands continuously and linearly into the depth of the material with increasing time. Gaining this information, the FIB-milled cross section investigations are most essential and the basis for further analyses.

No significant gradient is detectable in this layer, which ends up with a distinct border to the untreated bulk material with a roughness on the grain scale.

From these results, it is now possible to interpret the results of the XRD near-surface measurements correctly. This means that the transformation layer starts already consisting of a fixed amount of monoclinic ZrO_2 (the true saturation limit, which depends on the material) nearly from the very beginning and proceeds without growth restriction. Any reported so-called saturation limitations with time are only due to the limited individual penetration depth of the analytical tool used, e.g., XRD or Raman spectroscopy. With the direct investigation of the FIB cross sections via SEM, it is now possible to "translate" the quantified XRD results correctly into a real layer thickness, as long as the analytical setup and the aging parameters can be clearly distinguished.

The present authors envisage the kinetics to be controlled by the reaction velocity of water or its constituents with the rim of zirconia grains, which are contacted by water through unimpeded access within the transformed layer. The autocatalytic transformation of single grains opens the pathway into the depth of the material, where the reaction velocity again takes control.

Acknowledgements

The authors gratefully acknowledge support by the German Research Association DFG under contract Ni-299/23-1. They would like to thank VITA Zahnfabrik Rauter GmbH & Co. KG for kindly supplying the material used and the support in this study, Mr. Qu and Prof. Strunk (Institute for Materials Science, University Stuttgart) for the EBSD measurements, and Mr. Dreher and Mr. Kern at the NMI Reutlingen for offering their FIB/SEM equipment and their know-how.

Appendix A. Figures with essential colour discrimination

Certain figures in this article, particularly Figs. 8, 9, and 10 are difficult to interpret in black and white. The full colour images can be found in the on-line version, at http://dx.doi.org/10.1016/j.actbio.2012.08.032.

References

[1] Lilley E. Review of low temperature degradation in Y-TZPs. In: Tressler RE, McNallans M, editors. Corrosion and corrosive degradation of ceramics. Westerville, OH: American Ceramic Society; 1990. p. 387–407.
[2] Chevalier J, Gremillard L, Deville S. Low-temperature degradation of zirconia and implications for biomedical implants. Annu Rev Mater Res 2007;37(1):1–32.
[3] Lughi V, Sergo V. Low temperature degradation aging of zirconia: a critical review of the relevant aspects in dentistry. Dent Mater 2010;26(8):807–20.
[4] Murase Y, Kato E. Phase transformation of zirconia by ball-milling. J Am Ceram Soc – Discussions and notes 1979;62(9-10):527.
[5] Kosmac T, Oblak C, Jevnikar P, Funduk N, Marion L. Strength and reliability of surface treated Y-TZP dental ceramics. Appl Biomater 2000;53:304–13.
[6] Juy A, Anglada M. Surface phase transformation during grinding of Y-TZP. J Am Ceram Soc 2007;90(8):2618–21.
[7] Kao HC, Ho FY, Yang CC, Wei WJ. Surface machining of fine-grain Y-TZP. J Eur Ceram Soc 2000;20(14–15):2447–55.
[8] Borchers L et al. Influence of hydrothermal and mechanical conditions on the strength of zirconia. Acta Biomater 2010;6(12):4547–52.
[9] Chevalier J. Low-temperature aging of Y-TZP ceramics. J Am Ceram Soc 1999;82(8):2150–4.
[10] Kobayashi K, Kuwajima H, Masaki T. Phase change and mechanical properties of ZrO_2–Y_2O_3 solid electrolyte after ageing. Solid State Ionics 1981;3–4:489–93.
[11] Guo X. Property degradation of tetragonal zirconia induced by low-temperature defect reaction with water molecules. Chem Mater 2004;16:3988–94.
[12] Lawson S. Environmental degradation of zirconia ceramics. J Eur Ceram Soc 1995;15(6):485–502.
[13] Guo X. Hydrothermal degradation mechanism of tetragonal Zirconia. J Mater Sci 2001;36(15):3737–44.
[14] Guo X. On the degradation of zirconia ceramics during low-temperature annealing in water or water vapor. J Phys Chem Solids 1999;60(4):539–46.
[15] Johnson WA, Mehl RF. Reaction kinetics in processes of nucleation and growth. Trans Am Inst Min Metall Eng 1939;135:416–58.
[16] Whitney ED. Kinetics and mechanism of the transition of metastable tetragonal to monoclinic zirconia. Trans Faraday Soc 1965;61:1991–2000.
[17] Lu HY, Lin HY, Chen SY. Autocatalytic effect and microstructural development during ageing of 3 mol% Y_2O_3–TZP. Ceram Int 1987;13(4):207–14.
[18] Lawson S, Smith PA. A new technique for monitoring aging in yttria–tetragonal zirconia polycrystals. J Am Ceram Soc 1993;76(12):3170–2.
[19] Gremillard L, Chevalier J, Epicier T, Deville S, Fantozzi G. Modeling the aging kinetics of zirconia ceramics. J Eur Ceram Soc 2004;24(13):3483–9.
[20] Cattani-Lorente M, Scherrer SS, Ammann P, Jobin M, Wiskott HWA. Low temperature degradation of a Y-TZP dental ceramic. Acta Biomater 2011;7(2):858–65.
[21] Nakajima K, Kobayashi K, Murata Y. Phase stability of Y-PSZ in aqueous solutions. Adv Ceram 1984;12:399.
[22] Marro F, Anglada M. Strengthening of vickers indented 3Y-TZP by hydrothermal ageing. J Eur Ceram Soc 2012;32:317–24.
[23] Marro F, Armas Z, Horwat D, Anglada M. Estimation of thickness of hydrothermal degraded layer in 3Y-TZP by X-ray diffraction. IOP Publishing; 2009.
[24] Muñoz-Tabares J, Jiménez-Piqué E, Anglada M. Subsurface evaluation of hydrothermal degradation of zirconia. Acta Mater 2011;59(2):473–84.
[25] Muñoz-Tabares J, Jiménez-Piqué E, Reyes-Gasga J, Anglada M. Microstructural changes in ground 3Y-TZP and their effect on mechanical properties. Acta Mater 2011;59:6670–83.
[26] Chowdhury S, Vohra YK, Lemons JE, Ueno M, Ikeda J. Accelerating aging of zirconia femoral head implants: change of surface structure and mechanical properties. J Biomed Mater Res Part B: Appl Biomater 2007;81(2):486–92.
[27] Wada S, Yokoyama K. Differences in the tetragonal to monoclinic phase transformation rate in hot water of 3 mol% Y_2O_3–ZrO_2 ceramics under different surface conditions. Nippon seramikkusu kyokai gakujutsu ronbunshi 1999;107(1):92–5.
[28] Sato T, Shimada M. Control of the tetragonal-to-monoclinic phase transformation of yttria partially stabilized zirconia in hot water. J Mater Sci 1985;20(11):3988–92.
[29] Sato T, Shimada M. Transformation of yttria-doped tetragonal ZrO_2 polycrystals by annealing in water. J Am Ceram Soc 1985;68:356–9.
[30] Wulfman C, Djaker N, Dupont N, Ruse D, Sadoun M, la Chapelle ML. Raman spectroscopy evaluation of subsurface hydrothermal degradation of zirconia. J Am Ceram Soc 2012;95(7):2347–51.
[31] Kosmač T, Kocjan A. Ageing of dental zirconia ceramics. J Eur Ceram Soc 2012;32:2613–22.
[32] Kim YS, Jung CH, Park JY. Low temperature degradation of yttria-stabilized tetragonal zirconia polycrystals under aqueous solutions. J Nucl Mater 1994;209(3):326–31.
[33] Berthold C, Bjeoumikhov A, Brügemann L. Fast XRD^2 microdiffraction with focusing X-ray microlenses. Part Part Syst Char 2009;26:107–11.
[34] Beer A. Bestimmung der Absorption des rothen Lichts in farbigen Flüssigkeiten. Annalen der Physik 1852;162:78–88.
[35] Garvie RC, Nicholson PS. Phase analysis in zirconia systems. J Am Ceram Soc 1972;55(6):303–5.
[36] Toraya H, Yoshimura M, Somiya S. Calibration curve for quantitative analysis of the monoclinic-tetragonal ZrO_2 system by X-ray diffraction. J Am Ceram Soc 1984;67(6):C-119–C-121.
[37] Keuper M. Nachweis der oberflächennahen Phasenumwandlung von Zirkoniumdioxid: Vergleich von Raman Spektroskopie und XRD. Diploma thesis, Tübingen: Eberhard Karls Universität; 2009.
[38] Eder K. Niedertemperaturumwandlung in dentalen Zirkoniumdioxid Keramiken: Charakterisierung und Einfluss der Farbgebung. Diploma thesis, Tübingen: Eberhard Karls Universität; 2012.
[39] Marro FG, Chintapalli R, Hvizdos P, Soldera F, Mucklich F, Anglada M. Study of near surface changes in yttria-doped tetragonal zirconia after low temperature degradation. Int J Mater Res 2009;100(1):92–6.

[40] Soldera F, Gaillard Y, Gomila M, Muecklich F. FIB-tomography of nanoindentation cracks in zirconia polycrystals. Microsc Microanal 2007;13(S02):1510–1.
[41] De Grauw CJ, Sijtsema NM, Otto C, Grewe J. Axial resolution of confocal Raman microscopes: Gaussian beam theory and practice. J Microsc 1997;188(Part 3):237–79.
[42] Everall N. Confocal Raman microscopy: why the depth resolution and spatial accuracy can be much worse than you think. Appl Spectrosc 2000;54(10): 1515–20.
[43] Presser V, Keuper M, Berthold C, Nickel KG. Experimental determination of the Raman sampling depth in ZrO_2 ceramics. J Appl Spectrosc 2009;63(11): 1288–92.
[44] Dorn M, Nickel KG. Zirconia ceramics: phase transitions and raman spectroscopy. In: Gogotsi Y, Domnichs S, editors. High pressure surface science and engineering. Bristol: Institute of Physics Publishing; 2004. p. 466–519.
[45] Gaillard Y, Jimenez-Piqué E, Soldera F, Mücklich F, Anglada M. Quantification of hydrothermal degradation in zirconia by nanoindentation. Acta Mater 2008;56:4206–16.
[46] Gremillard L, Grandjean S, Chevalier J. A new method to measure monoclinic depth profile in zirconia-based ceramics from X-ray diffraction data. Int J Mater Res 2010;101(1):88–94.
[47] Lepistö T, Mäntylä T. A model for structural degradation of Y-TZP ceramics in humid atmosphere. In: 13th annual conference on composites and advanced ceramic materials. Tampere University of Technology Institute of Materials Science Tampere, Finland. Wiley-American Ceramic Society; 2009.
[48] Tsukuma K. Mechanical properties and thermal stability of CeO_2 containing tetragonal zirconia polycrystals. Am Ceram Soc Bull 1986;65(10).
[49] Lepistö TT, Lintula PV, Mäntylä TA. TZP-ceramics in humid conditions at 150 °C. Wiley Online Library; 1988.